IDENTIFICATION OF GTN DAMAGE PARAMETERS AS A SURROGATE MODEL FOR S355

RUI YAN[1], HAOHUI XIN[1]* and MILAN VELJKOVIC[1]

[1] *Faculty of Civil Engineering & Geosciences, Delft University of Technology, the Netherlands*
E-mail: H.Xin@tudelft.nl

The accurate simulation of ductile fracture becomes a more important role in the simulation to improve the validity of predicting structural behavior of hollow section joints. Gurson-Tvergaard-Needleman (GTN) damage model is used in this paper as a surrogate fracture simulation approach. The pressure dependency on the deviatoric stress is investigated based on computational homogenization methods. The inelastic deformations within the unit cell included with random spherical pores are analyzed for different types of loading conditions with respect to different stress triaxiality levels. The parameters q_1, q_2, and q_3 in the GTN yield surface are fitted based on the two-scale homogenized results. The proposed parameters for based material, the critical value of the void volume fraction f_c and the value of void volume fraction at which there is a complete loss of stress carrying resistance in the material f_f are calibrated by the results of coupon tests from the literature. A good agreement is observed, indicating the model and fitted parameters in this paper could be effectively used in the finite element simulation of the hollow section joints.

Keywords: Structural Steel; Gurson-Tvergaard-Needleman (GTN) Damage Model; Triaxiality; Two-scale homogenization.

1 Introduction

The accurate predicting of ductile fracture becomes very important in predicting of the ultimate state of hollow section joints. Proper modelling of the weld material, the heat affected zone and the base material are crucial and a systematic approach is lacking in presently available literature. Properties for material modelling of each component will be addressed using the surrogate model for different steel grades in an on-going project at TUD, planned together with Tampere University of Technology, Finland. The localization of the plasticity in the necking zone is overestimated by traditional elastoplastic hardening model if material damage is not considered (Zhang 1994, Ling 2004). Traditional approach for material modelling was used for the joints of rectangular sections with high strength steel (ROUSTE 2016). If the damage evolution of the material is considered (Pavlovic 2015, Yan 2019), a good agreement of finite element analysis and the experimental results is obtained. In this paper, a preliminary study is performed on S355 specimens cut from plate, as reported in Tu (2016) to examine the concept for ductile fracture modelling. The failure mechanism of ductile steels is growth and coalescence of micro voids (Benzerga and Jean-Baptiste 2010) which nucleate at inclusions or second-phase particles by particle-matrix interface de-cohesion or particle cracking. A widely used model linking the macroscopic damage with an evolution of micro void volume fraction growth is proposed by Gurson (1977), which is further improved by Tvergaard (1982) and Needleman and

Proceedings of the 17th International Symposium on Tubular Structures.
Editors: X.D. Qian and Y.S. Choo

Published by Research Publishing, Singapore.
ISBN: 978-981-11-0745-0; doi:10.3850/978-981-11-0745-0_066-cd

Tvergaard (1987) to consider void nucleation and coalescence, known as Gurson-Tvergaard-Needleman (GTN) Damage Model.

A variety of material specimens can be used to determine the fracture process such as smooth, notched bars or compact tension specimens where the experimental fracture properties and failure modes are varied to examine the effects of stress triaxiality and Lode Angles (Kiran and Khandelwal 2013). One test series including many samples need to be involved to identify the parameters of the damage model. In addition to experiments, numerical micromechanical analysis are useful in calibrating the parameters of ductile fracture models. Fritzen et al. (2012) calibrates the parameters for elastoplastic porous metals by using a three-dimensional (3D) porous volume elements. Xin et al. (2017) identifies the material parameters of orthotropic GTN model inferred from microstructures generated from the high-fidelity discrete element simulations. Xin et al. (2019) calibrates the friction angle, the ratio of the yield stress in triaxial tension to the yield stress in triaxial compression and the dilation angle of the linear Drucker-Prager plastic model based on experimental results and computational homogenization.

In this paper, GTN damage model is used as a surrogate fracture simulation approach. The pressure dependency on the deviatoric stress is investigated based on computational homogenization methods. The inelastic deformations within the unit cell included with random spherical pores are analyzed for different types of loading conditions with respect to different stress triaxiality levels. The parameters q_1, q_2, and q_3 in the GTN yield surface are fitted based on the two-scale homogenized results. The proposed parameters for base material, the critical value of the void volume fraction f_c and the value of void volume fraction at which there is a complete loss of stress carrying resistance in the material f_f is calibrated by the results of coupon tests from the literature (Tu 2016). Very good agreement of FEA and experiments is obtained. The same approach is applying in the on-going research project on tubular joints made of cold-formed steel grades S355, S500 and S700.

2 Material models

2.1 *GTN model*

The yield surface of GTN model is shown in Eq. 1 (Needleman and Tvergaard 1987):

$$\phi = \left(\frac{\sigma_{eq}}{\sigma_y}\right)^2 + 2q_1 f^* \cosh\left(\frac{3q_2\sigma_m}{2\sigma_y}\right) - 1 - q_3 f^{*2} = 0 \tag{1}$$

Where: q_1, q_2, and q_3 are the constitutive parameters, σ_{eq}, σ_m and σ_y are the von Mises equivalent stress, the hydrostatic pressure and the flow stress of the undamaged material matrix respectively. σ_{eq} and σ_m can be calculated by following equations:

$$\sigma_m = \frac{1}{3}\sigma_{ij}\delta_{ij} \tag{2}$$

$$\sigma_{\text{eq}} = \sqrt{\frac{3}{2}\left(\sigma_{ij} - \frac{1}{3}\sigma_{ij}\delta_{ij}\right)\left(\sigma_{ij} - \frac{1}{3}\sigma_{ij}\delta_{ij}\right)} \tag{3}$$

f^* is a function of the critical volume fraction f_c and final void volume fraction f_f, and is expressed as following (Needleman and Tvergaard 1987):

$$f^* = \begin{cases} f & f < f_c \\ f_c + K\left(f - f_c\right) & f_c \le f < f_f \\ f_u^* & f \ge f_f \end{cases} \qquad K = \frac{f_u^* - f_c}{f_f - f_c} \tag{4}$$

The change in void volume fraction during an increment of deformation process contains two parts: one due to the growth of existing voids and the other due to the nucleation of new voids (Needleman and Tvergaard 1987):

$$\dot{f} = \dot{f}_g + \dot{f}_n \tag{5}$$

Growth of existing voids is based on the law of conservation of mass and is expressed as:

$$\dot{f}_g = \left(1 - f\right)\dot{\varepsilon}_{kk}^{pl} \tag{6}$$

Nucleation of voids may occur due to microcracking and/or decohesion of the particle-matrix interface:

$$\dot{f}_n = A\dot{\varepsilon}_{eq}^{pl} \tag{7}$$

$$A = \frac{f_n}{S_n\sqrt{2\pi}} e\wedge\left[-\frac{1}{2}\left(\frac{\varepsilon_{eq}^{pl} - \varepsilon_n}{S_n}\right)^2\right] \tag{8}$$

where: f_n is the void volume fraction of the nucleated void; ε_n is the mean value of the normal distribution of the nucleation strain; S_n is the standard deviation.

2.2 Periodic Boundary Condition

The micro-scale and macro-scale behavior could be associated by Hill-Mandel Computational Homogenization. The Cauchy stress σ_{ij} in macro-scale level could be calculated by averaging the Cauchy stress $\tilde{\sigma}_{ij}$ in the unit cell domain (Fish 2013).

$$\sigma_{ij} = \frac{1}{\Theta}\int_{\Theta} \tilde{\sigma}_{ij} d\Theta \tag{9}$$

The displacement in micro-scale level $u_i^f(x, y)$ could be given by leading order translation-free micro-scale displacement which depends on the stain tensors in the macro-scale domain ε_{ij}^c, perturbation displacement of the micro-scale $u_i^{(1)}(x, y)$, position vector in macro-scale x and macro-scale level y, expressed as below (Fish 2013):

$$u_i^f(x, y) = \varepsilon_{ij}^c y_j + u_i^{(1)}(x, y) \tag{10}$$

Periodic boundary conditions could apply the same perturbation displacement to a pair of Master and Slave nodes located at the opposite faces. Thus, the following relation which could be realized by constraint equations between a Master node and a Slave node as follows:

$$u_i^f(x, y_j^M) - u_i^f(x, y_j^S) = \varepsilon_{ij}^c\left(y_j^M - y_j^S\right) \tag{11}$$

2.3 Uniaxial stress-strain relationship

The non-linear isotropic hardening model presented in the ABAQUS software(2014) is used to consider the plasticity of steel. A linear combination of a power and an exponential law (Roth 2016) is employed to model uniaxial stress-strain relationship of the structural steel S355.

$$\sigma_{\varepsilon}\left[\bar{\varepsilon}_p\right]=\alpha\sigma_{\mathrm{S}}\left[\bar{\varepsilon}_p\right]+\left(1-\alpha\right)\sigma_{\mathrm{V}}\left[\bar{\varepsilon}_p\right] \tag{12}$$

Where: α is the weighting factor. The power law (Swift, 1952)

$$\sigma_{\mathrm{S}}\left[\bar{\varepsilon}_p\right]=A\left(\bar{\varepsilon}_p+\varepsilon_0\right)^n \tag{13}$$

Where: $A,\ \varepsilon_0,\ n$ are the Swift parameters. The exponential law (Voce, 1948)

$$\sigma_{\mathrm{V}}\left[\bar{\varepsilon}_p\right]=k_0+Q\left(1-e^{-\beta\bar{\varepsilon}_p}\right) \tag{14}$$

Where: $k_0,\ Q,\ \beta$ are the Voce parameters.

3 Finite element model

3.1 *Material Property*

The material property of matrix is reproduced from the literature (Tu 2016) where tensile tests are performed based on EN 10002-1(2001) at room temperature. The Young's modulus is 207.75GPa and the Poisson ratio is 0.3. A linear combination of a power law and an exponential law is used to treat the material's strain hardening behavior after necking for matching the micro homogenization results to macro material properties. The fitted and calibrated parameters are given in Table 1 and the true stress-plastic strain curve is shown in Figure 1 where the experimental data only includes data before the ultimate stress.

Table 1. Plasticity model parameters for S355

α	A[MPa]	ε_0	n	k_0 [MPa]	Q [MPa]	β
0.6	935.9	0	0.2075	302	328	19.9

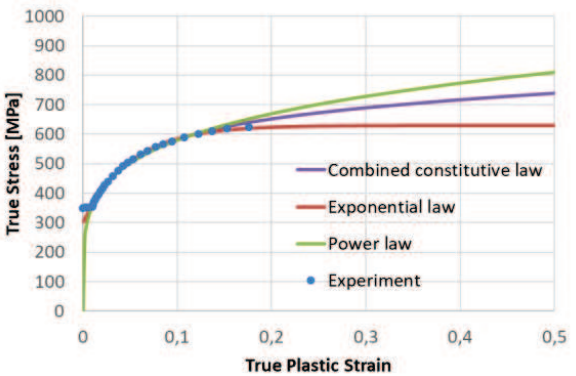

Figure 1. True stress- plastic strain curve

3.2 *Unit Cell Generation*

Six finite element unit cell models with different void volume fractions f varifying from 0.0663% to 25% are built to identify the parameters in the yield surface of GTN model. Typical unit cell with random voids is shown in Fig. 2. The number of the random non-overlapping voids with constant radius N within the unit cell are varying from 10 to 80 depending on the size of the voids. The void volume fraction f of the unit cell is calculated by following equations:

$$f = 4\pi NR^3 / \left|\Omega_{tot}\right| / 3 \tag{15}$$

Where: $\left|\Omega_{tot}\right|$ is the total volume of the unit cell. Since the side length of the cubic unit cell is 1mm, the volume of the unit cell is 1mm^3 in this paper. The details including voids number, radius and porosity of unit cell are listed in Table 2.

Table 2. Details of microstructures

f(%)	0.0663	1.5	3	5	10	25
N	10	40	40	40	80	80
R (mm)	0.0251	0.0447	0.0564	0.0668	0.0668	0.0907

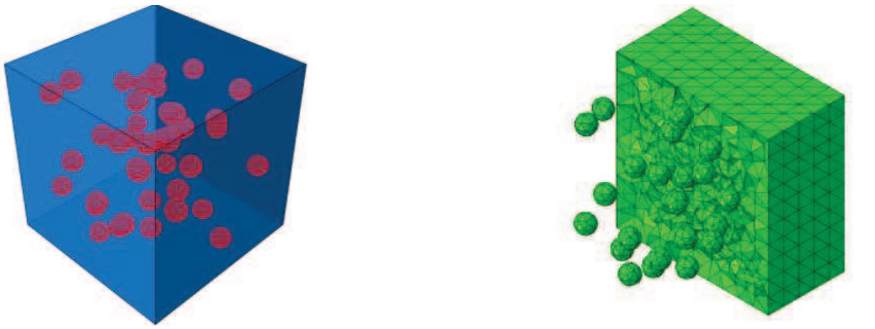

a) N=40, *f*=3%

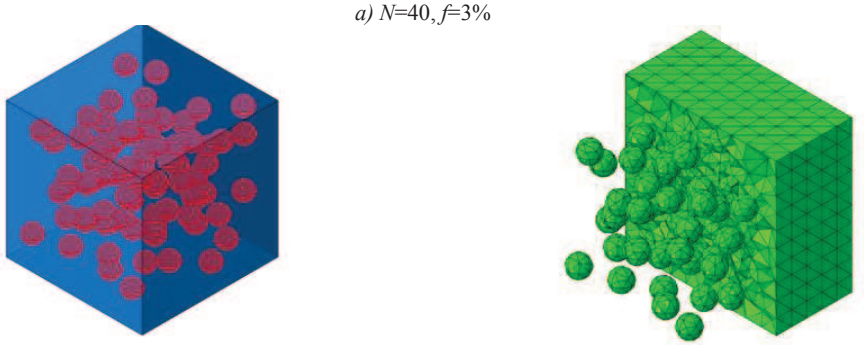

b) *N*=80, *f*=10%

Figure 2. Typical unit cell model with random voids

3.3 *Boundary Conditions*

The parameters q_1, q_2, and q_3 in the GTN model, which reflect the hydrostatic pressure dependency of the macroscopic yield surface, are generally investigated by varying macroscopic stress triaxiality. A total of 14 loading conditions, listed in Table 3, are used to varying stress triaxiality by changing two parameters α and β proposed by Fritzen et al. (2012). The strain-driven boundary conditions are shown below:

$$\left[\dot{\bar{\varepsilon}}\right]=\alpha\begin{pmatrix}1&0&0\\0&-1&0\\0&0&0\end{pmatrix}+\beta\begin{pmatrix}1&0&0\\0&1&0\\0&0&1\end{pmatrix} \tag{9}$$

Table 3. Parameters for different load conditions

i	1	2	3	4	5	6	7	8	9	10	11	12	13	14
α	1	1	1	1	1	1	1	1	1	1	1	1	1	1
β	0.05	0.1	0.2	0.3	0.5	0.7	0.9	1.2	1.4	1.6	1.8	2.0	3.0	5.0

4 Simulation results

4.1 *Parameters identification of yield surface*

An example of the Mises stress- hydrostatic pressure curves extracted from the model with 5% volume void fraction under load conditions 3,5,7,9,12 and 14 in Table 3 are given in Figure 3. The results show that a larger β leads to a smaller Mises stress, and the Mises stress increases in the beginning and decreases later with the increasing of hydrostatic pressure. Fig.4 shows the relationship between the yield strength and the hydrostatic pressure with the same porosity. The parameters of the yield surface are fitted per each porosity, and the results are listed in Table 4. In addition, q_1=1.62 and q_2=0.97 are proposed by applying the least square method considering different void volume fractions.

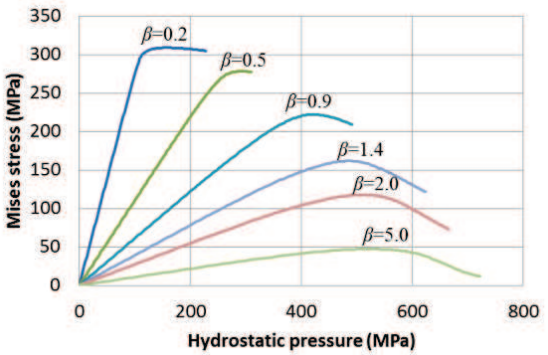

Figure 3. Typical Mises stress- hydrostatic pressure relationship (f=5%, α=1)

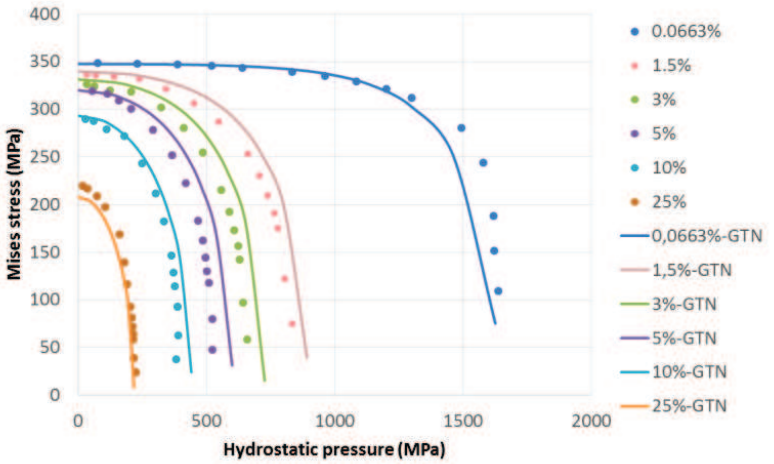

Figure 4. Relationship between yield strength and hydrostatic pressure with same porosity

Table 4. Parameters of yield surface for different porosity

$f_{nominal}$ (%)	0.0663	1.5	3	5	10	25
f_{EVOL} (%)	0.0656	1.46	2.95	4.98	9.71	24.8
q_1	1.00±0.78	1.70±0.16	1.73±0.10	1.51±0.13	1.54±0.19	1.44±0.04
q_2	1.01±0.11	1.01±0.03	1.03±0.02	1.13±0.03	1.10±0.07	1.07±0.03
R^2	0.961	0.994	0.995	0.991	0.965	0.987

4.2 *Parameters calibration of damage evolution*

The damage evolution parameters f_c and f_f are calibrated through test results of the notched round bars reported by Tu (2016) as shown in Figure 6. Note that the void nucleation parameters ε_n, f_n and s_n is based on Tu (2016). The initial void volume fraction f_0 is obtained according to Franklin's formula (1969) as 0.063%. The calibration process is proceeded by comparing load versus elongation (ΔL) curves and load versus cross section diameters reduction (ΔD) curves. After the parametric study, the FE results with parameters f_c=0.04 and f_f=0.25 show a good agreement with experimental results. Three critical points are marked and the maximum voids volume fractions (VVF) are shown in Fig. 7. Point A corresponds to the maximum stress, and the maximum VVF is around 0.44%. At the Point B, obvious degradation is observed and the VVF (4.0%) at point B generally equals to f_c. The point C corresponds to fracture point, and the VVF (25.0 %) is the value of f_f. The values of parameters in GTN model for S355 are proposed in Table 5.

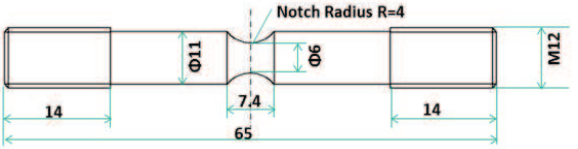

Figure 6. Geometry of the notched bar (Tu 2016)

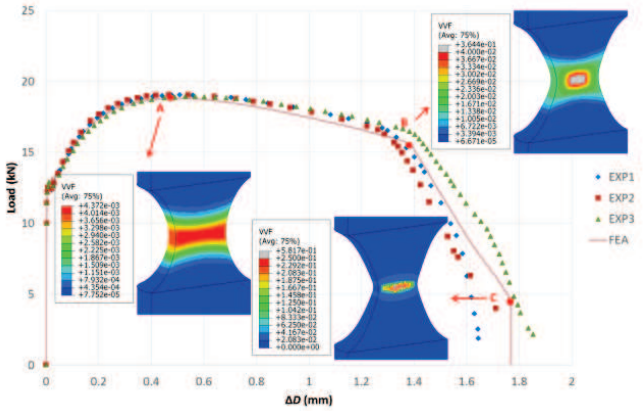

(a) Load-ΔL curve

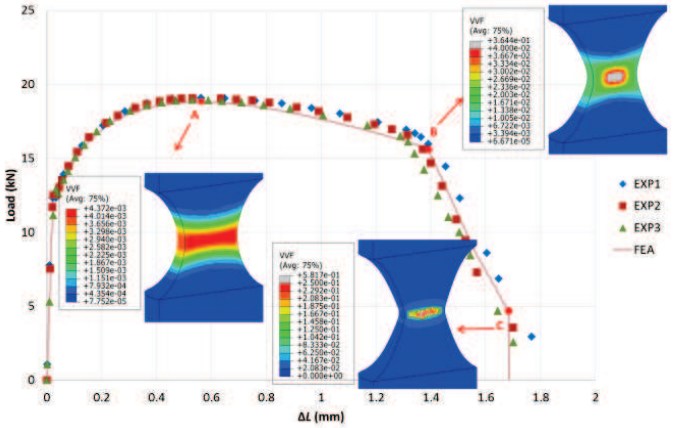

(b) Load-Δ*D* curve

Figure 7. Comparison between FE and test results

Table 5. Proposed parameters for the GTN model

q_1	q_2	q_3	f_0	f_c	f_f	ε_n	f_n	s_n
1.62	0.97	2.62	6.63E-4	0.04	0.25	0.2	0.01	0.1

5 Conclusions

In this paper, Gurson-Tvergaard-Needleman (GTN) damage model is used in this paper as a surrogate fracture simulation approach. The parameters q_1, q_2, and q_3 of the yield surface is identified via computational homogenization methods. The damage evolution parameters f_c and f_f are calibrated by the experimental results of notched round bars. The value of f_c corresponds to the VVF at obvious degradation (Point B in Fig. 7) and the value f_f equals to the VVF at failure point (Point C in Fig. 7). The values of parameters in GTN model for S355, tested by Tu (2016) are proposed. A good agreement is observed between the results of simulation and experiments in the tensile tests of the notched round bars.